PAPER

CrossMark
click for updates

5-Arylpyrimido-[4,5-*b*]quinoline-diones as new and sustainable corrosion inhibitors for mild steel in 1 M HCl: a combined experimental and theoretical approach†

Chandrabhan Verma,[a] L. O. Olasunkanmi,[bc] I. B. Obot,[d] Eno E. Ebenso[bc] and M. A. Quraishi*[a]

The inhibition of mild steel corrosion in 1 M HCl by four 5-arylpyrimido-[4,5-*b*]quinoline-diones (APQDs), namely 5-(4-nitrophenyl)-5,10-dihydropyrimido [4,5-*b*]quinoline-2,4(1*H*,3*H*)-dione (**APQD-1**), 5-phenyl-5,10-dihydropyrimido[4,5-*b*]quinoline-2,4(1*H*,3*H*)-dione (**APQD-2**), 5-(4-hydroxyphenyl)-5,10-dihydropyrimido-[4,5-*b*]quinoline-2,4(1*H*,3*H*)-dione (**APQD-3**) and 5-(2,4-dihydroxyphenyl)-5,10-dihydropyrimido[4,5-*b*]quinoline-2,4(1*H*,3*H*)-dione (**APQD-4**) has been investigated using weight loss, electrochemical, surface, and quantum chemical calculations and molecular dynamics simulation methods. The results showed that the inhibition efficiency (η%) increased with increasing concentration of the inhibitors. Among the studied compounds, **APQD-4** exhibited the highest inhibition efficiency of 98.30% at 20 mg l^{-1} concentration. The studied compounds effectively retarded the corrosion of mild steel in 1 M HCl by adsorbing onto the steel surface, and the adsorption data conformed to the Langmuir adsorption isotherm. The results of potentiodynamic polarization measurements revealed that the studied compounds are cathodic-type inhibitors. Scanning electron microscopy (SEM) study confirmed the formation of adsorbed films of the inhibitor molecules on the steel surface. Quantum chemical calculations and molecular dynamics simulations were undertaken to corroborate experimental findings and provide adequate insight into the corrosion inhibition mechanisms and adsorption characteristics of the studied compounds.

1. Introduction

Metals and alloys undergo chemical and/or electrochemical reactions with the environment to form relatively more stable compounds and consequently there is a loss of metals due to the corrosion process. Among different available methods that have been identified for corrosion control, the use of synthetic corrosion inhibitors is one of the most appropriate, effective and economic ways of mitigating corrosion problem.[1–4] However, most of the synthetic corrosion inhibitors are toxic and not environmentally friendly. In recent years, green

chemistry has attracted considerable attention from synthetic and medicinal chemists due to increasing ecological awareness and strict environmental regulation.[5,6] Therefore, the current trend of research in corrosion inhibition is directed towards the development of green corrosion inhibitors that offer high inhibition efficiency at low environmental risk.[7,8] In this regard, multicomponent reactions have immerged as a green and powerful technique in synthetic organic chemistry and drug discovery in the sense that several biologically active complexes/ molecules can be synthesized in one step by using commercially available cheap starting materials.[9,10] The multicomponent reactions have several advantages such as operational simplicity, facile automation and minimized waste generation, because of the reduction in the number of work-up, extraction and purification stages.[11,12] Furthermore, the consumption of environmentally benign solvents and chemicals during the reactions provides the means of upholding the essential principles of green chemistry. Nowadays, the development of synthetically useful reactions using water as reaction medium has drawn considerable attention because of its non-flammable, non-hazardous, non-toxic, uniquely redox-stable, inexpensive and free availability.[13–15] Moreover, in asymmetric organocatalysis, the use of proline, particularly in water and

aDepartment of Chemistry, Indian Institute of Technology, Banaras Hindu University, Varanasi 221005, India. E-mail: maquraishi.apc@itbhu.ac.in; maquraishi@ rediffmail.com; Fax: +91-542-2368428; Tel: +91-9307025126

bDepartment of Chemistry, School of Mathematical & Physical Sciences, Faculty of Agriculture, Science and Technology, North-West University (Mafikeng Campus), Private Bag X2046, Mmabatho 2735, South Africa

cMaterial Science Innovation & Modelling (MaSIM) Research Focus Area, Faculty of Agriculture, Science and Technology, North-West University (Mafikeng Campus), Private Bag X2046, Mmabatho 2735, South Africa

dCenter of Research Excellence in Corrosion, Research Institute, King Fahd University of Petroleum and Minerals, Dhahran 31261, Saudi Arabia

† Electronic supplementary information (ESI) available. See DOI: 10.1039/c5ra27417f

ionic liquids is the most sustainable alternative method as it is directly isolated from natural biological sources without using any hazardous chemical and/or solvents such as DMSO, DMF and other chlorinated solvents.[16–18] Literature survey reveals that quinoline and aryl pyrimidine as well as their derivatives possesses potential applications in the synthesis of pharmacologically active compounds. These derivatives have been used as anti-microbial, analgesic, anti-viral, anti-inflammatory, anti-HIV, anti-tubercular, anti-tumor, anti-neoplastic, anti-malaria, diuretic, cardiovascular agents DNA binding capabilities, anti-tumor, DNA-intercalating carrier *etc.*[19–21]

In view of this, the present work reported the corrosion inhibition efficiency of four 5-aryl-pyrimido[4,5-*b*]quinoline-dione derivatives (APQDs) on mild steel in 1 M HCl using weight loss, electrochemical impedance spectroscopy (EIS), potentiodynamic polarization, scanning electron microscopy (SEM), quantum chemical calculations and molecular dynamics simulation methods. The novelty of the work is that the 5-arylpyrimido-[4,5-*b*]quinoline-diones (APQDs) and similar compounds have not been previously investigated as metallic corrosion inhibition. Further, a careful survey of literature revealed that 5-arylpyrimido-[4,5-*b*]quinoline-diones derivatives synthesized in our lab, those consist of fused quinoline and aryl pyrimidine moieties, showed better inhibition efficiency than quinoline[22–24] and aryl pyrimidine[25–28] derivatives synthesized and investigated by other researchers, which further implies that the APQDs can be considered as novel corrosion inhibitors. The higher inhibition efficiencies of the investigated inhibitors are attributed due to the presence of aromatic rings and double bonds in addition to the several nitrogen (N) and oxygen (O) atoms those act as adsorption centers. The choice of these compounds as corrosion inhibitors was based on the fact that they can: (a) be easily synthesized using green starting materials with high yield, (b) exhibit high inhibition efficiency even at very low concentrations, (c) strongly adsorb on metal surface through several heteroatoms in the form of polar functional groups (–OH –NO$_2$, –CN, –NH$_2$) and aromatic rings, thereby inhibit corrosion effectively, and (d) easily dissolve in test solutions due to the presence of various polar functional groups.

2.   Experimental procedures

2.1.   Materials

2.1.1.   Synthesis of 5-arylpyrimido-[4,5-*b*]quinoline-diones (APQDs). As described earlier,[29] a mixture comprising of aniline (1 mmol), aldehyde (1 mmol), barbituric acid (1 mmol), and ʟ-proline catalyst (0.05 g, 20 mol%) in water (2 ml) was refluxed for 12 h. The completion of reactions and formation of products were checked by TLC method. After completion of reaction, the reaction mixtures were cooled to room temperature and the resulting solid crude products were filtered. The solid crude precipitates were washed with water (10 ml) and finally with ethanol (5 ml) to obtain pure 5-arylpyrimido-[4,5-*b*] quinoline-diones (APQDs). The synthesized inhibitors were characterized by physical and spectroscopic analysis. The characterization data of the synthesized compounds are given

in Table 1. The synthetic scheme for the studied APQDs is shown in Fig. 1.

2.1.2.   Electrodes and reagents. The working electrodes were cut from the commercially available mild steel sheet having chemical composition (wt%): C (0.076), Mn (0.192), P (0.012), Si (0.026), Cr (0.050), Al (0.023), and Fe (balance). The exposed surface of the working electrode was cleaned successively with emery papers of different grade (600, 800, 1000, 1200), washed with double distilled water, degreased with acetone, ultrasonically cleaned with ethanol before being used for weight loss and electrochemical experiments. The test solution (1 M HCl) was prepared by appropriately diluting the hydrochloric acid (HCl, 37%, Merck) using double distilled. The volume of the electrolyte (1 M HCl) was 100 ml for weight loss and electrochemical measurements.

2.2.   Methods

2.2.1.   Weight loss measurements. The cleaned, dried and accurately weighted mild steel specimens having dimension 2.5 × 2.0 × 0.025 cm^3 were immersed in 100 ml of 1 M HCl without and with different concentrations of APQDs for 3 h. After the elapsed time, the specimens were removed, washed with distilled water and acetone, dried in moisture free desiccator, and then weighted accurately. Each experiment was performed in triplicate to insure reproducibility, and the mean values of weight loss were recorded. The inhibition efficiency ($\eta\%$) was calculated from the average weight loss values using expression:[30,31]
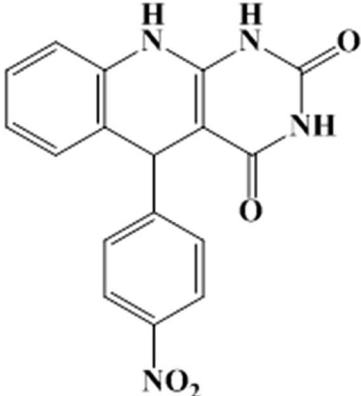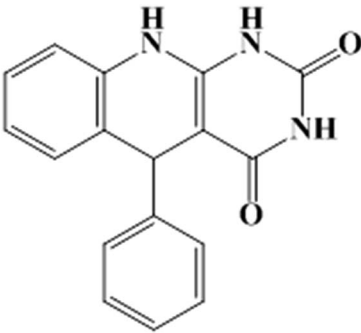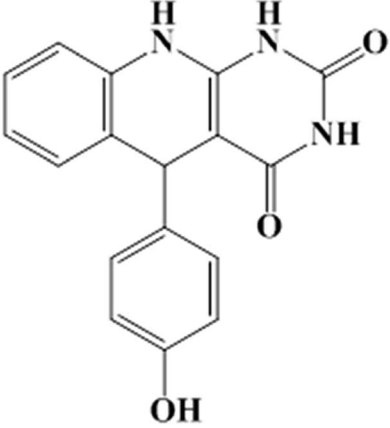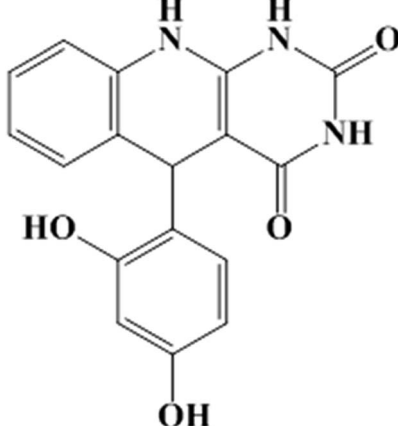
$$\eta\% = \frac{w_\text{o} - w_\text{i}}{w_\text{o}} \times 100 \qquad (1)$$

where w_o and w_i are the weight loss values without and with various concentrations of APQDs (the inhibitors), respectively.

2.2.2.   Electrochemical measurements. The mild steel specimens with exposed surface area of 1 cm^2 (one sided) were utilized for all electrochemical measurements under potentiodynamic condition using the Gamry Potentiostat/Galvanostat (Model G-300) instrument. Gamry Echem Analyst 5.0 software was used to fit and analyze all electrochemical data. A three-electrode electrochemical cell consisting of mild steel as working electrode (WE), platinum as counter electrode and a saturated calomel electrode (SCE) as reference electrode was used for all the electrochemical measurements. Before starting the electrochemical experiments, the working electrode was allowed to corrode freely for sufficient time in order to attain steady open circuit potential (OCP). During polarization measurements, the cathodic and anodic Tafel slopes were recorded by changing the electrode potential from −0.25 to +0.25 V *vs.* corrosion potential (E_corr) at a constant sweep rate of 1.0 mV s^{-1}. The corrosion current density (i_corr) was determined by extrapolating the linear segments of the Tafel slopes (cathodic and anodic). The inhibition efficiency was calculated from the i_corr values by using the relation:[30,31]

$$\eta\% = \frac{i_\text{corr}^0 - i_\text{corr}^\text{i}}{i_\text{corr}^0} \times 100 \qquad (2)$$

Table 1 IUPAC name, molecular structure, molecular formula, melting point and analytical data of studied APQDs

| S. no.	IUPAC name and abbreviation of inhibitor	Chemical structure	Molecular formula and M.P. and analytical data
1	5-(4-Nitrophenyl)-5,10-dihydropyrimido-[4,5-*b*]quinoline-2,4(1*H*,3*H*)-dione (**APQD-1**)		$C_{17}H_{12}N_4O_4$ (mol. wt. 336.30), white colored solid, IR spectrum (KBr cm^{-1}): 3556, 3448, 3427, 2842, 1694, 1646, 1536, 1422, 1328, 1093, 858, 624; ^{1}H NMR (300 MHz, DMSO) δ (ppm): 6.12, 7.22, 7.37–7.43, 7.96–8.07, 10.23–10.42
2	5-Phenyl-5,10-dihydropyrimido-[4,5-*b*]quinoline-2,4(1*H*,3*H*)-dione (**APQD-2**)		$C_{17}H_{13}N_3O_2$ (mol. wt. 291.30), white creamy solid, IR spectrum (KBr cm^{-1}): 3687, 3574, 3454, 3024, 1680, 1646, 1436, 1402, 1298, 1226, 1163, 786, 742, 718, 628; ^{1}H NMR (300 MHz, DMSO) δ (ppm): 5.96–6.21, 6.96, 7.11–7.23, 7.54, 8.09, 9.45, 10.83–10.92
3	5-(4-Hydroxyphenyl)-5,10-dihydropyrimido[4,5-*b*]quinoline-2,4(1*H*,3*H*)-dione (**APQD-3**)		$C_{17}H_{13}N_3O_3$ (mol. wt. 307.30), creamy colored solid, IR spectrum (KBr cm^{-1}): 3785, 3678, 3582, 1686, 1571, 1456, 1270, 1204, 1168, 1098, 966, 872, 784, 698; ^{1}H NMR (300 MHz, DMSO) δ (ppm): 5.46, 6.73–682, 7.67, 7.96, 8.36, 9.42, 10.76, 12.04–12.13
4	5-(2,4-Dihydroxyphenyl)-5,10-dihydropyrimido[4,5-*b*]quinoline-2,4(1*H*,3*H*)-dione (**APQD-4**)		$C_{17}H_{13}N_3O_4$ (mol. wt. 323.30), yellowish solid, IR spectrum (KBr cm^{-1}): 3843, 3762, 3549, 3428, 2864, 1669, 1627, 1542, 1484, 1436, 1254, 1198, 1045, 958, 679, 624; ^{1}H NMR (300 MHz, DMSO) δ (ppm): 5.36, 6.59, 6.98–7.11, 7.43, 7.96, 8.56, 9.71, 12.45–12.54
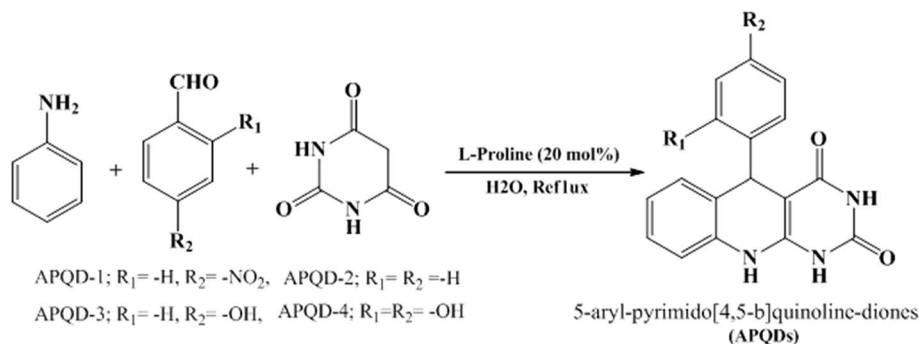
Fig. 1 Synthetic route of studied APQDs.

where i_{corr}^0 and i_{corr}^i are corrosion current in the absence and presence of different concentrations of APQDs, respectively.

Electrochemical impedance measurements were carried out at the OCP in the frequency range of 100 kHz to 0.01 Hz using AC signal of amplitude 10 mV peak-to-peak. The charge transfer resistances were calculated from the obtained Nyquist plots. The inhibition efficiency was calculated using the equation:[30,31]

$$\eta\% = \frac{R_{ct}^i - R_{ct}^0}{R_{ct}^i} \times 100 \qquad (3)$$

where, R_{corr}^0 and R_{corr}^i are charge transfer resistances in absence and presence of different concentrations of APQDs, respectively.

2.2.3. SEM measurements. For surface analysis, the cleaned mild steel specimens of the above mentioned composition were allowed to corrode for 3 h in the absence and presence of optimum concentration of the studied APQDs. Thereafter, the specimens were retrieved, washed with water, dried and used for SEM. The SEM model Ziess Evo 50 XVP was used to investigate the micromorphology of mild steel surface at 500× magnification.

2.2.4. Quantum chemical calculations. Quantum chemical calculations were carried out on the studied compounds using the density functional theory (DFT) method involving the Becke three-parameter hybrid functional together with the Lee–Yang–Paar correlation functional (B3LYP).[32–34] The 6-31+G(d,p) basis set was chosen for all the calculations. All the calculations were carried out with the aid of Gaussian 09 software for Windows (Revision D.01).[35] The gas phase optimized geometries of the compounds were confirmed to correspond to their true energy minima by the absence of imaginary frequency in the computed vibrational frequencies. All quantum chemical parameters were derived based on the electronic parameters of the most stable conformers of the molecules. The frontier molecular orbital (FMO) energies, that is, the highest occupied molecular orbital energy (E_{HOMO}) and the lowest unoccupied molecular energy (E_{LUMO}) were calculated. Other parameters such as the energy gap (ΔE), global electronegativity (χ), and the fraction of electrons transfer from the inhibitor to the metal atom were computed respectively according to the equations:[36,37]

$$\Delta E = E_{LUMO} - E_{HOMO} \qquad (4)$$

Table 2 The weight loss parameters obtained for mild steel in 1 M HCl containing different concentrations of APQDs[a]

Inhibitor	Conc (mg l^{-1})	Weight loss (mg)	C_R (mg cm^{-2} h^{-1})	Inhibition efficiency ($\eta\%$)	Surface coverage (θ)
Blank	0.0	230	7.66	—	—
APQD-1	5	104	3.46	54.78	0.5478
	10	50	1.66	78.26	0.7826
	15	28	0.93	87.82	0.8782
	20	18	0.60	92.17	0.9217
APQD-2	5	88	2.93	61.73	0.6173
	10	40	1.33	82.60	0.826
	15	22	0.73	90.43	0.9043
	20	14	0.46	93.91	0.9391
APQD-3	5	81	2.70	64.78	0.6478
	10	32	1.06	86.08	0.8608
	15	17	0.56	92.60	0.926
	20	11	0.33	95.65	0.9565
APQD-4	5	68	2.26	70.43	0.7043
	10	26	0.86	88.69	0.8869
	15	13	0.43	94.34	0.9434
	20	8	0.26	96.52	0.9652

[a] Standard deviation: 0.00025 to 0.0003.

$$\chi = -\frac{1}{2}(E_{\text{LUMO}} + E_{\text{HOMO}}) \tag{5}$$

$$\Delta N = \frac{\chi_{\text{Fe}} - \chi_{\text{inh}}}{2(\eta_{\text{Fe}} + \eta_{\text{inh}})} \tag{6}$$

where χ_{Fe} and η_{inh} denote the electronegativity and hardness of iron and inhibitor respectively. A value of 7 eV mol^{-1} was used for the χ_{Fe}, while η_{Fe} was taken as 0 eV mol^{-1} for bulk Fe atom in accordance with the Pearson's electronegativity scale.[38]

The Fukui functions f^+ and f^- are local reactivity indices that are often used to analyze the relative susceptibility of the active atomic sites of an inhibitor molecule to electrophilic and nucleophilic attacks respectively.[37,39,40] The atom condensed Fukui functions using the Mullikan population analysis (MPA) and the finite difference (FD) approximations approach introduced by Yang and Mortier[37,41] were calculated as:

$$f_{\text{k}}^+ = \rho_{\text{k}(N+1)}(r) - \rho_{\text{k}(N)}(r) \tag{7}$$

$$f_{\text{k}}^- = \rho_{\text{k}(N)}(r) - \rho_{\text{k}(N-1)}(r) \tag{8}$$

where f_{k}^+ and f_{k}^- are the electrophilic and nucleophilic Fukui indices respectively condensed on atom k, while $\rho_{\text{k}(N+1)}$, $\rho_{\text{k}(N)}$ and $\rho_{\text{k}(N-1)}$ are the electron densities of the $(N+1)$-, (N)- and $(N-1)$-electron systems respectively approximated by the Mulliken gross charges. The electron density surfaces of the f_{k}^+ and f_{k}^- were visualized using the Multiwfn software.[42,43]

2.2.5. Molecular dynamics (MD) simulations. The molecular dynamics (MD) simulations were performed using Forcite module in the Material Studio Software 7.0 from BIOVIA-Accelrys, USA. Fe (110) surface was chosen for the simulation since it is the most stable crystal surface of Fe.[44] The simulation was carried out with Fe (110) crystal with a slab of 5 Å in depth using periodic boundary conditions, in order to simulate a representative part of an interface devoid of any arbitrary boundary effects. The Fe (110) plane was then enlarged to a (8 × 8) supercell to provide a large surface for the interactions with the inhibitors. A vacuum slab of 30 Å thickness was then built above the Fe (110) plane. The Fe (110) surface was fixed before simulations. For the whole simulation procedure, the Condensed-phase Optimized Molecular Potentials for Atomistic Simulation Studies (COMPASS) force field was used to optimize the structures of all components of the system of interest. The MD simulations were performed in NVT canonical ensemble at 298 K with applied settings of vdw & Coulomb, a cut-off radius of 15.5 Å, a time step of 0.1 fs and a total simulation time of 100 ps using Anderson thermostat. A total of 1 000 000 number of simulation steps was carried out.

The interaction energy ($E_{\text{interaction}}$) of molecules with Fe surface was obtained using the equation:[45]

$$E_{\text{interaction}} = E_{\text{total}} - (E_{\text{Fe surface}} + E_{\text{molecule}}) \tag{9}$$

where E_{total} is the total energy of the molecules and the metal surface system; E_{surface} is defined as the energy of metal surface without adsorption of molecules and E_{molecule} is the energy of isolated molecules. The binding energy is the negative of the interaction energy and is given as:

$$E_{\text{binding}} = -E_{\text{interaction}} \tag{10}$$

3. Results and discussion

3.1. Weight loss experiments

3.1.1. Effect of concentration. Due to the operational simplicity and good reliability of weight loss experiment, the effect of different concentrations of APQDs on mild steel corrosion in 1 M HCl was first studied by this method at 308 K for an immersion time of 3 h. Each weight loss experiment was performed in triplicate and the data showed good reproducibility with standard deviation ranging from 0 to 0.00025. The values of weight loss parameters such as corrosion rate (C_{R}), inhibition efficiency ($\eta\%$), and surface coverage (θ) obtained from weight loss measurements are given in Table 2. The weight loss measurements show that $\eta\%$ increases with increasing concentration for all the inhibitors and attains a maximum value of 92.17% for **APQD-1**, 95.21% for **APQD-2**, 96.52% for **APQD-3**, and 97.82 for **APQD-4**, at 20 mg l^{-1}. Further increase in concentration did not cause any significant change in the inhibition performance suggesting that 20 mg l^{-1} is the optimum concentration. An increase in APQDs concentration beyond 20 mg l^{-1}, the inhibitor molecules adsorb onto the metallic surface perpendicularly because of the electrostatic repulsion function at higher concentration.[46] And therefore, compared with paralleled adsorption, adsorbed inhibitor molecules with perpendicular adsorption would occupy either similar or even smaller surface area which resulted in no any

Table 3 Variation of C_{R} and $\eta\%$ with temperature in absence and presence of optimum concentration of APQDs in 1 M HCl[a]

	Corrosion rate (C_{R}) (mg cm^{-2} h^{-1}) and inhibition efficiency ($\eta\%$)									
	Blank		APQD-1		APQD-2		APQD-3		APQD-4	
Temperature (K)	C_{R}	$\eta\%$	C_{R}	$\eta\%$	C_{R}	$\eta\%$	C_{R}	$\eta\%$	C_{R}	$\eta\%$
308	7.66	—	0.60	92.16	0.46	93.99	0.33	95.69	0.26	96.60
318	11.0	—	1.36	87.63	1.13	89.72	0.90	91.81	0.73	93.36
328	14.3	—	2.60	81.81	2.23	84.40	1.90	86.71	1.63	88.60
338	18.6	—	5.20	72.04	4.73	74.56	4.46	76.02	4.06	78.17

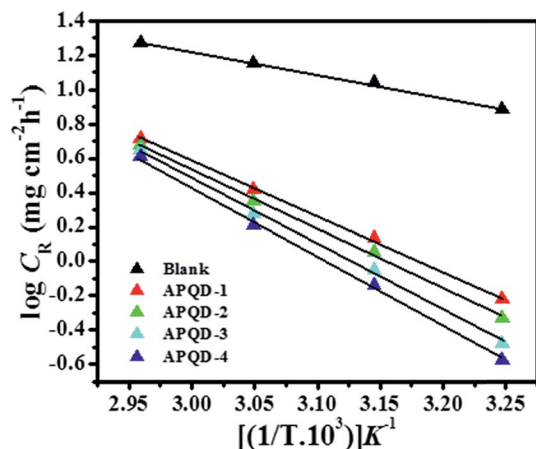[a] Standard deviation: 0.00025 to 0.0003.

Fig. 2 Arrhenius plots for the corrosion of mild steel in 1 M HCl.

significant change in the inhibition performance beyond 20 mg l^{-1} concentration.[47,48] The increased inhibition efficiency upon increasing concentration of APQDs is attributed to increase in the extent of surface coverage by the inhibitor molecules. From the weight loss results it is observed that the inhibition efficiency of the studied APQDs follows the order: **APQD-4** > **APQD-3** > **APQD-2** > **APQD-1**. The lower inhibition efficiency of the **APQD-1** despite its more number of N and O atoms compared to **APQD-2** could be as a result of electron withdrawing nature of the nitrophenyl group at position 5 of the pyrimido-quinoline-dione ring, which decreases the electron density on the adjacent phenyl rings. Conversely, the high inhibition performances of the **APQD-3** and **APQD-4** can be attributed to the electron releasing effect of the hydroxyl phenyl group(s) at position 5 of the pyrimido-quinoline-dione ring which increases the electron density over the adjacent rings. Previously, it has been reported by several researchers that the presence of electron withdrawing groups (such as $-NO_2$) in inhibitor molecules decreases the inhibition performance.[49,74] While, presence of electron releasing groups (such as $-OH$, $-NH_2$, $-OCH_3$) in the inhibitor molecules increases the inhibition efficiency.[50,74] It is obvious from the structure of **APQD-4** that it has two addition electron releasing hydroxyl ($-OH$) groups at second and fourth position of the aromatic ring of aldehydic moiety which resulted into high electron density in form of four addition lone pair of

Table 4 Values of activation energies for mild steel dissolution in 1 M HCl in the absence and at of optimum concentration of APQDs[a]

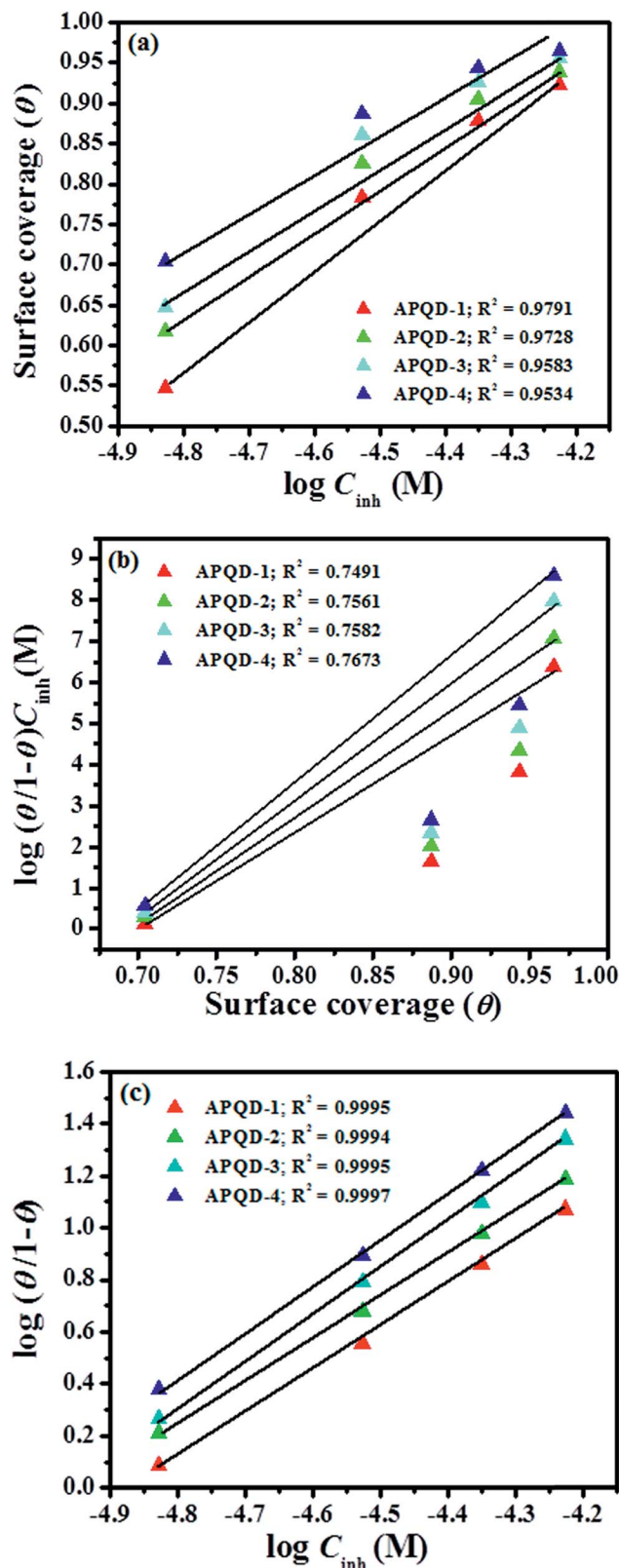| Inhibitor	E_a (kJ mol^{-1})
Blank	28.48
APQD-1	61.52
APQD-2	65.88
APQD-3	73.70
APQD-4	77.49

[a] Standard deviation: 0.00025 to 0.0003.

Fig. 3 (a) Temkin, (b) Frumkin, and (c) Langmuir adsorption isotherm plots for the adsorption of APQDs on mild steel surface in 1 M HCl.

electrons those further increased the adsorption and highest inhibition efficiency of **APQD-4** among the tested compounds.

3.1.2.   Effect of temperature. The influence of temperature was studied by performing the weight loss experiments in the absence and presence of optimum concentrations of the APQDs for 3 h immersion time in the temperature range of 308–338 K. The values of the inhibition efficiency ($\eta\%$) and corrosion rate (C_R) derived from the weight loss experiments at different temperatures are presented in Table 3. From the results depicted in Table 3 it is seen that an increase in temperature causes significant decrease in the $\eta\%$ and increase in the C_R. The decreased $\eta\%$ and increased C_R with increasing temperatures may due to desorption of the adsorbed inhibitor molecules leading to greater surface area of mild steel getting in contact with the acidic solution.[51,52] Moreover, rapid etching, desorption, and decomposition and/or rearrangement of inhibitor molecules might also be responsible for the decrease in the inhibition performance at elevated temperatures.[50] The temperature dependency of C_R can be expressed with the aid of Arrhenius equation, where the natural logarithm of C_R is a linear function of $1/T$:[53,54]

$$\log(C_R) = \frac{-E_a}{2.303RT} + \log A \qquad (11)$$

where C_R is the corrosion rate in mg cm^{-2} h^{-1}, A is the Arrhenius pre-exponential factor, R is the gas constant and T is absolute temperature. The values of E_a were calculated from the slope of Arrhenius plots ($-\Delta E_a/2.303R$) (Fig. 2) for all studied APQDs and the results are presented in Table 4. Obviously, the values of activation energy are higher in the presence of the APQDs ranging from 55.47 to 90.49 kJ mol^{-1} compared to 28.48 kJ mol^{-1} observed in the absence of the inhibitors. A larger increase in activation energy is observed for the more efficient inhibitor. The higher values of E_a suggested that more energy barrier have been achieved in presence of inhibitors and the rate of mild steel dissolution is reduced due to the formation of inhibitors–Fe complex.[55]

3.1.3.   Adsorption isotherm. Adsorption isotherm is very important in corrosion inhibition studies for the purpose of investigating the nature/mechanism and the rapidity/strength of the adsorption process. The adsorption isotherms provide structural as well as thermodynamic information of the adsorbed double layer. Several commonly used isotherms, namely

Table 5 The values of K_{ads} and ΔG°_{ads} for mild steel in absence and presence of optimum concentration of APQDs in 1 M HCl at different studied temperature[a]

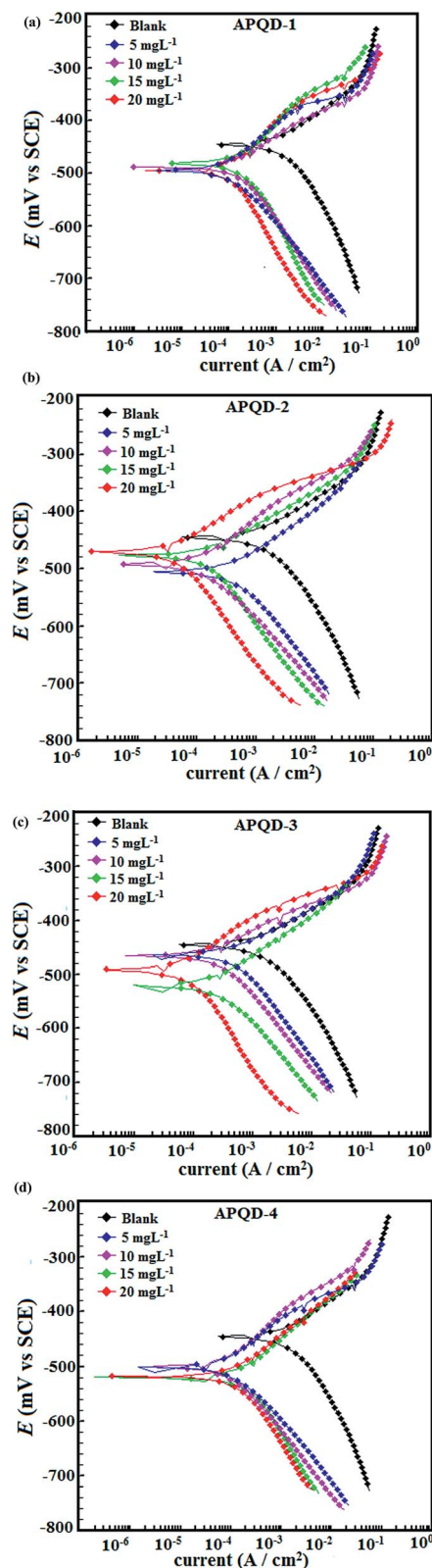| Inhibitor	K_{ads} (10^4 M^{-1})				$-\Delta G^\circ_{ads}$ (kJ mol^{-1})			
	308	318	328	338	308	318	328	338
APQD-1	1.60	0.84	0.54	0.31	35.09	34.53	34.40	33.89
APQD-2	1.85	1.04	0.65	0.35	35.45	35.09	34.90	34.25
APQD-3	2.63	1.34	0.78	0.38	36.36	35.76	35.42	34.47
APQD-4	3.32	1.67	0.93	0.43	36.96	36.35	35.89	34.81

[a] Standard deviation: 0.00025 to 0.0003.

Fig. 4 Polarization curves for mild in the absence and presence of different concentrations of (a) **APQD-1**, (b) **APQD-2**, (c) **APQD-3**, and (d) **APQD-4**.

Langmuir, Frumkin, and Temkin were tested among which the Langmuir isotherm showed the best fit with regression coefficient (R^2) values close to unity for all studied compounds. The Temkin, Frumkin, and Langmuir isotherms plots are given in Fig. 3. Careful examination of the Fig. 3 shows that among the tested isotherms, the Langmuir isotherm gave the best fit because in this case the values of R^2 are most close to unity for all inhibitors whereas for Frumkin and Temkin isotherms, the values of R^2 were much apart from unity. Further, although the values of R^2 in Langmuir adsorption isotherm were close to one, the considerable deviation of the slope from unity indicated that the Langmuir isotherm could not be strictly applied. The deviation of slope values from unity is attributed due to inter-molecular interactions of adsorbed species which causes mutual repulsion or attraction.[56,57] Moreover, the deviation of the slope could also be a result of the changes in the adsorption heat with increasing surface coverage which has not been considered during derivation of Langmuir adsorption isotherm.[58] The Langmuir adsorption isotherm can be expressed as:[59]

$$K_{ads}C = \frac{\theta}{1 - \theta} \tag{12}$$

where K_{ads} is the equilibrium constant of the adsorption process, C is the inhibitor concentration and θ is the surface coverage. The value of equilibrium constant, K_{ads} was calculated from the intercept of the straight line of the Langmuir isotherm plots for all studied compounds at different temperatures. The standard free energy of adsorption (ΔG_{ads}°), is related to the K_{ads} by the equation:

$$\Delta G_{ads}^{\circ} = -RT \ln(55.5 K_{ads}) \tag{13}$$

The numerical value 55.5 represents the molar concentration of water in acid solution. The calculated values of K_{ads} and

ΔG_{ads}° at each studied temperature in presence of optimum concentration of APQDs are given in Table 5. In general, values of ΔG_{ads}° up to -20 kJ mol^{-1} or more positive are consistent with electrostatic interactions taking place between the charged inhibitor molecules and the charged metal surface (physisorption), while those around -40 kJ mol^{-1} or less positive are assumed to involve the sharing of charges between the inhibitor molecules and the metal surface to form a coordinate type of bond (chemisorption).[60,61] In the present study, the large negative values of ΔG_{ads}° (-33.31 kJ mol^{-1} to -38.19 kJ mol^{-1}) for the investigated inhibitors suggest that the inhibitors can adsorb spontaneously on mild steel surface to form highly stable adsorption film.[62,63] Furthermore, the observed range of ΔG_{ads}° values suggests that the adsorption of the inhibitors on mild steel surface is of "mixed mode", which implies that the adsorption of the studied inhibitors on mild steel in 1 M HCl solution involves both, physisorption and chemisorption processes.[63,64]

3.2. Electrochemical measurements

3.2.1. Polarization measurements. The potentiodynamic polarization measurements were undertaken in order to study the effect of investigated inhibitors (APQDs) on the anodic mild steel dissolution and cathodic hydrogen evolution reactions. The polarization curves for mild steel dissolution in the absence and presence of different concentrations of the studied inhibitors are shown in Fig. 4. Extrapolation of the linear segments of cathodic and anodic Tafel curves furnished essential corrosion parameters such as corrosion potential (E_{corr}), corrosion current density (i_{corr}) and anodic and cathodic Tafel slopes (β_a and β_c respectively). These polarization parameters along with calculated inhibition efficiency ($\eta\%$) are presented in Table 6. Examination of the results in Table 6 shows that with the addition of inhibitors to the acid solution, the values of i_{corr} decreases significantly with slight shift in the values of E_{corr}.

Table 6 Tafel polarization parameters for mild steel in 1 M HCl solution in absence and presence of different concentrations of APQDs

| Inhibitor	Conc (mg l^{-1})	E_{corr} (mV/SCE)	β_a (μA cm^{-2})	β_c (mV dec^{-1})	i_{corr} (mV dec^{-1})	$\eta\%$	θ
Blank	—	−445	70.5	114.6	1150	—	—
APQD-1	5	−492	83.7	162.3	489.6	57.42	0.5742
	10	−486	93.8	209.3	263.5	77.08	0.7708
	15	−478	55.6	100.3	146.4	87.26	0.8726
	20	−494	70.3	125.8	84.6	92.64	0.9264
APQD-2	5	−505	82.2	115.8	430.7	62.54	0.6254
	10	−493	65.9	156.9	173.4	84.92	0.8492
	15	−477	83.6	93.8	109.2	90.50	0.9050
	20	−471	71.5	126.7	58.6	94.90	0.9490
APQD-3	5	−464	70.5	111.6	397.3	65.45	0.6545
	10	−466	95.5	152.3	142.7	87.59	0.8759
	15	−521	53.8	54.7	78.6	93.16	0.9316
	20	−496	38.5	35.9	42.8	96.27	0.9627
APQD-4	5	−501	79.3	93.6	346.4	69.87	0.6987
	10	−505	94.4	109.3	132.6	88.46	0.8846
	15	−518	64.1	47.9	90.4	92.13	0.9213
	20	−520	38.5	35.9	23.7	97.93	0.9793
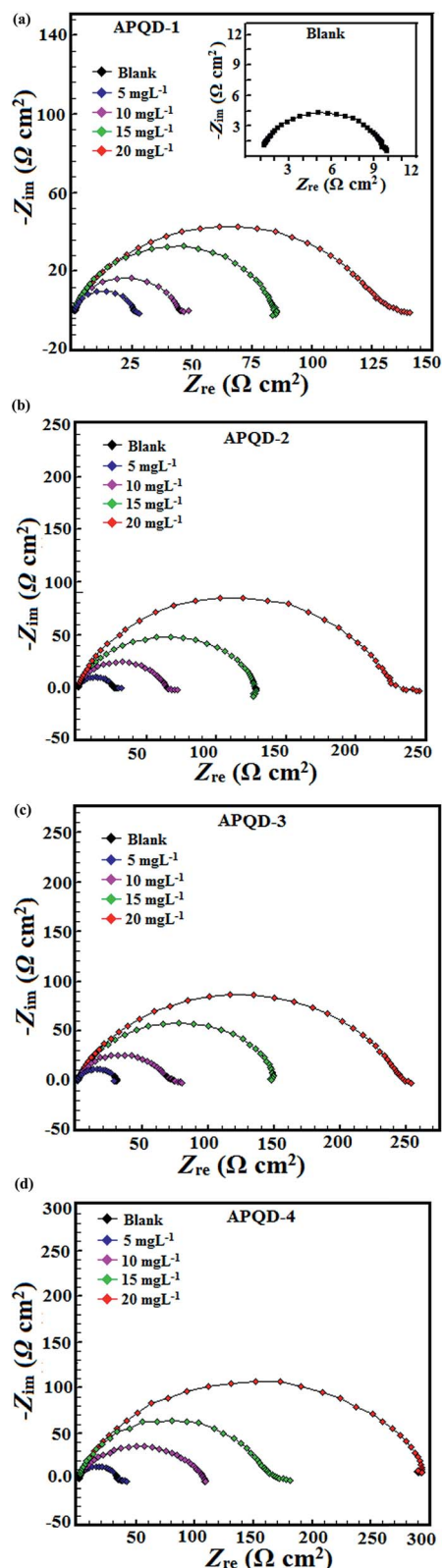
Fig. 5 Nyquist plot for mild steel in 1 M HCl in the absence and presence of different concentrations of (a) **APQD-1**, (b) **APQD-2**, (c) **APQD-3**, and (d) **APQD-4**.

The maximum shift in the value of E_{corr} in the present study was 75 mV which is less than 85 mV. Therefore, the studied compounds can be classified as mixed-type inhibitors, which implies the inhibitors reduce the anodic mild steel dissolution and also retard the cathodic hydrogen evolution reactions.[65–67] From the results depicted in Table 6 it is also noted that in presence of APQDs, the values of both β_a and β_c change irregularly but the change in values of β_c is somewhat more prominent compared to that of β_a suggesting that studied compounds act as mixed-type inhibitors but predominantly cathodic inhibitive.

3.2.2. Electrochemical impedance spectroscopy (EIS) studies. The effect of the synthesized compounds on the corrosion behavior of mild steel in 1 M HCl was also investigated by means of EIS method. The Nyquist plots obtained for mild steel in 1 M HCl in the absence and presence of different concentrations of the studied inhibitors are shown in Fig. 5. It is obvious that the EIS spectra of the inhibitors free solution and the EIS spectra of the inhibitors containing solutions show similar characteristics suggesting that mechanism of mild steel corrosion is similar in both the cases. The impedance spectra at different concentrations of the investigated APQDs showed single capacitive loop which suggests that the adsorption of these inhibitors takes place through simple surface coverage and the studied APQDs behave as primary interface inhibitors.[68] It is also evident from Fig. 5 that the diameter of the Nyquist plots increases with increasing inhibitors concentration which is attributed to the formation of protective film on mild steel surface leading to successful retardation of the corrosion process.[69] For a metallic system corroding in acid solution, the replacement of capacitance by CPE gives a better approximation.[70] CPE is defined in impedance representation as:

$$Z_{CPE} = \left(\frac{1}{Y_0}\right)[(jw)^n]^{-1} \tag{14}$$

where, Y_0 is the CPE constant, ω is the angular frequency; j is the imaginary number (*i.e.* $j^2 = -1$) and n is the phase shift (exponent) which is related to the degree of surface inhomogeneity. Depending on the value of n, CPE can represent resistance ($n = 0$, $Y_0 = R$), capacitance ($n = 1$, $Y_0 = C$), inductance ($n = -1$, $Y_0 = 1/L$) or Warburg impedance ($n = 0.5$, $Y_0 = W$). Where W is the Warburg parameter, the value of Warburg impedance (Z_W) related to the diffusion of the ions from the passive films of inhibitors. The values of the double layer capacitance (C_{dl}) in absence and presence of inhibitors were calculated from the equation:[71]

$$C_{dl} = Y_0(\omega_{max})^{n-1}$$

where, ω_{max} is the frequency at which the imaginary part of impedance has attained the maximum (rad s^{-1}) value. The impedance parameters were derived from the EIS spectra of the studied compounds using a previously described equivalent circuit,[72] and the results are presented in Table 7. A careful inspection of the data in Table 7 reveals that the presence of different concentrations of the studied inhibitors increases the

Table 7 EIS parameters obtained for mild steel in 1 M HCl in absence and presence of different concentrations of APQDs

Inhibitor	Conc (mg l^{-1})	R_s (Ω cm^2)	R_{ct} (Ω cm^2)	n	Y_0 (μF cm^{-2})	C_{dl} (μF cm^{-2})	$\eta\%$	θ
Blank	—	1.12	9.58	0.827	482.2	106.21	—	—
APQD-1	5	0.997	21.96	0.859	187.3	77.41	56.37	0.5637
	10	0.716	43.34	0.833	168.2	66.65	77.89	0.7789
	15	0.567	83.88	0.829	165.3	56.27	88.57	0.8857
	20	0.608	129.69	0.857	59.26	22.51	92.61	0.9261
APQD-2	5	0.844	25.25	0.837	156.3	56.54	62.05	0.6205
	10	0.96	62.82	0.857	114.8	51.74	84.75	0.8475
	15	0.83	125.67	0.846	84.95	33.12	92.37	0.9237
	20	0.766	232.03	0.842	56.42	21.12	95.87	0.9587
APQD-3	5	1.09	27.63	0.857	134.8	55.04	65.32	0.6532
	10	0.976	69.07	0.846	111.34	43.65	86.13	0.8613
	15	0.802	141.54	0.837	78.98	28.28	93.23	0.9323
	20	0.838	244.56	0.832	48.70	18.11	96.08	0.9608
APQD-4	5	0.922	33.42	0.869	124.21	54.56	71.33	0.7133
	10	0.98	104.12	0.856	113.80	42.99	90.79	0.9079
	15	0.82	166.58	0.842	72.30	24.75	94.24	0.9424
	20	0.819	295.38	0.836	43.81	16.79	96.75	0.9675

values of R_{ct} which could be as a result of increased surface coverage on mild steel by the inhibitor molecules.[73,74] It can be observed from the results depicted in Table 7 that the values of C_{dl} significantly decreased in the presence of various concentrations of the studied APQDs which could be as result of the decrease in dielectric constant and enhancement of the thickness of the electrical double layer. The values of 'n' are almost constant and close to unity suggesting that the interface is of capacitive characteristics.

The Bode angle plots recorded for the mild steel electrode immersed in 1 M HCl in the absence and presence of various concentrations of APQDs are shown in Fig. 6. As described earlier, the metal/electrolyte interface involved in present study is of a capacitive behaviour. An ideal capacitive behaviour would result in a slope value attains −1 and a phase angle value of −90°.[75] However, in our present study, in the intermediate frequency zone, a linear relationship between log|Z| $vs.$ log f with a slope near −0.84 and the phase angle approaching −70° has been observed. The deviation from the ideal capacitive behavior can be attributed to the roughness of electrode surface which occurred as a result of corrosion, and surface inhomogeneity attributable to structural and interfacial origin. However, examination of the Bode plots depicted in Fig. 6 reveals that the values of phase angle expressively increased due to formation of protective surface film. Furthermore, Bode plots give one time constant, sigma maxima in the intermediate frequency region. The broadening of this maximum in the Bode plots is attributed due to the adsorption and formation of protective film by inhibitors at the metal/electrolyte interface.

3.3. Surface measurements

3.3.1. Scanning electron microscopy (SEM). The SEM images of mild steel specimens exposed to 1 M HCl for 3 h in the absence and presence of optimum concentration of the investigated inhibitors are shown in Fig. 7. It can be seen from Fig. 7a that the mild steel surface was badly corroded and damaged due to free acid corrosion of the steel surface in absence of the inhibitors. However, in presence of the studied inhibitors, the surface morphology of the specimens was remarkably improved resulting in the observation of smoother and less corroded surfaces (Fig. 7b–e). The improved morphology of the mild steel surface is attributed to the formation of protective layer by the inhibitors over the metallic surface. This observation suggests that the APQDs used as corrosion inhibitors in the present study adsorb on mild steel surface and form protective film.

3.4. Theoretical measurements

3.4.1. Quantum chemical calculations. The optimized molecular structures and the respective HOMO and LUMO electron density surfaces of the studied compounds are shown in Fig. 8 and 9. The optimized structures showed that for all the four compounds, the substituted/unsubstituted phenyl group with which the molecules differ is not coplanar with the pyrimido-quinoline-dione ring. The HOMO electron density distribution provides information about the sites or fragments of the molecule that are most likely to donate electrons to the appropriate orbital of an acceptor specie, while the LUMO electron density distribution is a pointer to the sites of the molecule that possess higher chances of accepting electrons from a donor species.[76,79] As shown in Fig. 9, the electron density of the HOMO is delocalized over the entire molecular atoms/rings for **APQD-3** and **APQD-4**, while the 4-nitrophenyl group and the phenyl group at position 5 of the pyrimido-quinoline-dione ring in **APQD-1** and **APQD-2** respectively are not completely involved in the HOMO distributions. The involvement of the hydroxyl-substituted phenyl groups in **APQD-3** and **APQD-4** in the HOMO distribution is due to the electron donating effect of the hydroxyl group(s) adjacent to the phenyl ring. Similarly,
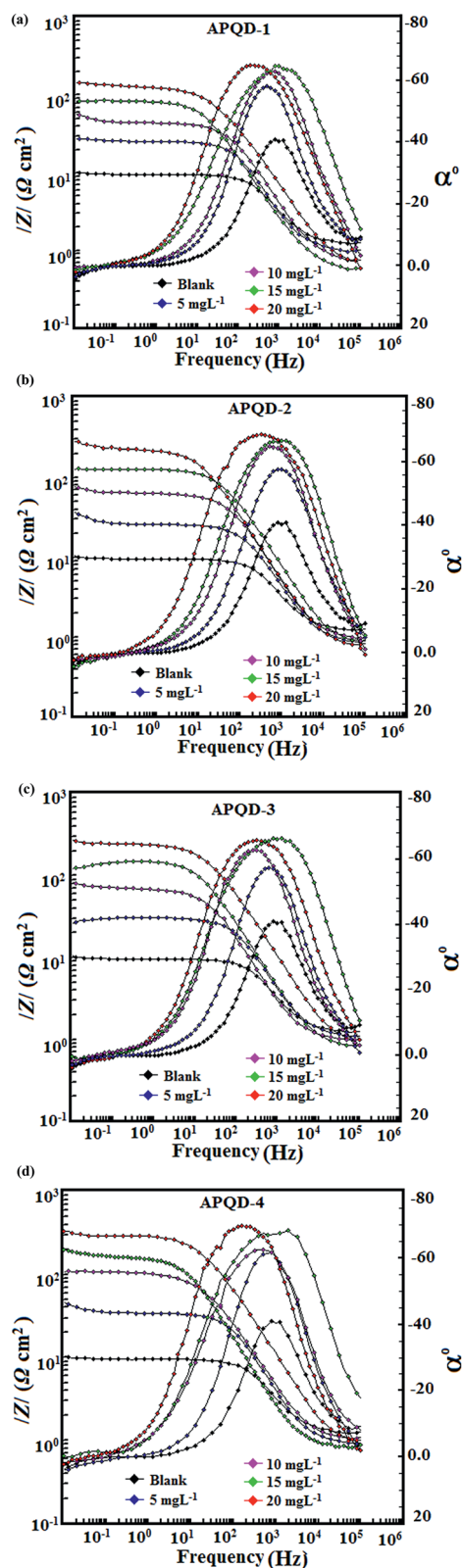
Fig. 6 Bode impedance modulus (log *f* vs. log|*Z*|) and phase angle (log *f* vs. α⁰) plots for mild steel in 1 M HCl in the absence and different of different concentrations of (a) **APQD-1**, (b) **APQD-2**, (c) **APQD-3**, and (d) **APQD-4**.

the low participation of the 4-nitrophenyl group in **APQD-1** in the HOMO electron density distribution is due to the electron withdrawing effect of the nitro group, which decreases the electron density on the adjacent phenyl ring.[72,79] This observation was also supported by the LUMO electron density distributions, which is concentrated on the 4-nitrophenyl group in **APQD-1**, indicating the high tendency of electron acceptance by the group. The LUMO is also completely delocalized over the entire pyrimido-quinoline-dione rings in **APQD-2**, **APQD-3** and **APQD-4** with somewhat reduced electron density on the atoms of the phenyl group. The –OH groups in **APQD-3** and **APQD-4** make very little contributions to the LUMO, which indicate that the molecules are not likely to accept electrons through these sites.

The values of some quantum chemical parameters for the studied compounds are listed in Table 8. The E_{HOMO} is a measure of the tendency of a molecule to donate its HOMO electrons to the appropriate vacant orbital of the receiving specie, such that the higher the E_{HOMO} the better the chance of electron donation by the molecule.[76,77] The values of the E_{HOMO} for the studied inhibitors are in the order: **APQD-4** > **APQD-3** > **APQD-2** > **APQD-1**, which agrees with the order of the experimental inhibition efficiencies (Table 8). The E_{LUMO} on the other hand is a measure of the affinity of a molecule to accept electrons to its LUMO, such that the lower the E_{LUMO} the higher the propensity of the inhibitor molecule to accept electrons from the appropriate occupied orbitals of iron. The results of the E_{LUMO} in Table 8 do not agree with the trend of the observed inhibition efficiencies. This suggests that the E_{LUMO} may not be a good descriptor for the relative inhibition efficiency of the studied molecules. The energy gap, ΔE is another index of reactivity of molecules for which a molecule with lower ΔE is usually more reactive and possesses higher inhibition efficiency.[78] The trend of the ΔE values obtained for the studied compounds is also not in agreement with the experimental inhibition efficiencies. The global electronegativity, χ is another reactivity index that predicts the extent to which a molecule holds on to its electrons. The higher the χ value the lower the chance of electron donation by the molecule and *vice versa*. The trend of the values of χ in Table 8 is **APQD-4**< **APQD-3**< **APQD-2**< **APQD-1**, which suggests that **APQD-4** has the highest possibility of donating electrons to an electrophilic center such as the iron surface that is populated by positive charges. The trend of χ is in agreement with the experimental inhibition efficiencies. The values of ΔN, the fraction of electrons transferred from the inhibitor molecule to the metal as reported in Table 8 also corroborate the trend of the experimental inhibition efficiencies. The ΔN values suggest that the fraction of electrons transferred from the inhibitor molecule to iron is in the order: **APQD-4** > **APQD-3** > **APQD-2** > **APQD-1**. All the quantum chemical parameters reported in Table 8 are in support of the assumption that the mode of adsorption of the studied molecules on the steel surface is predominantly *via* electron donation from the high electron density sites of the molecules to the iron. This assumption is also related to the fact that the surface of mild steel in acidic medium is reportedly populated by positive
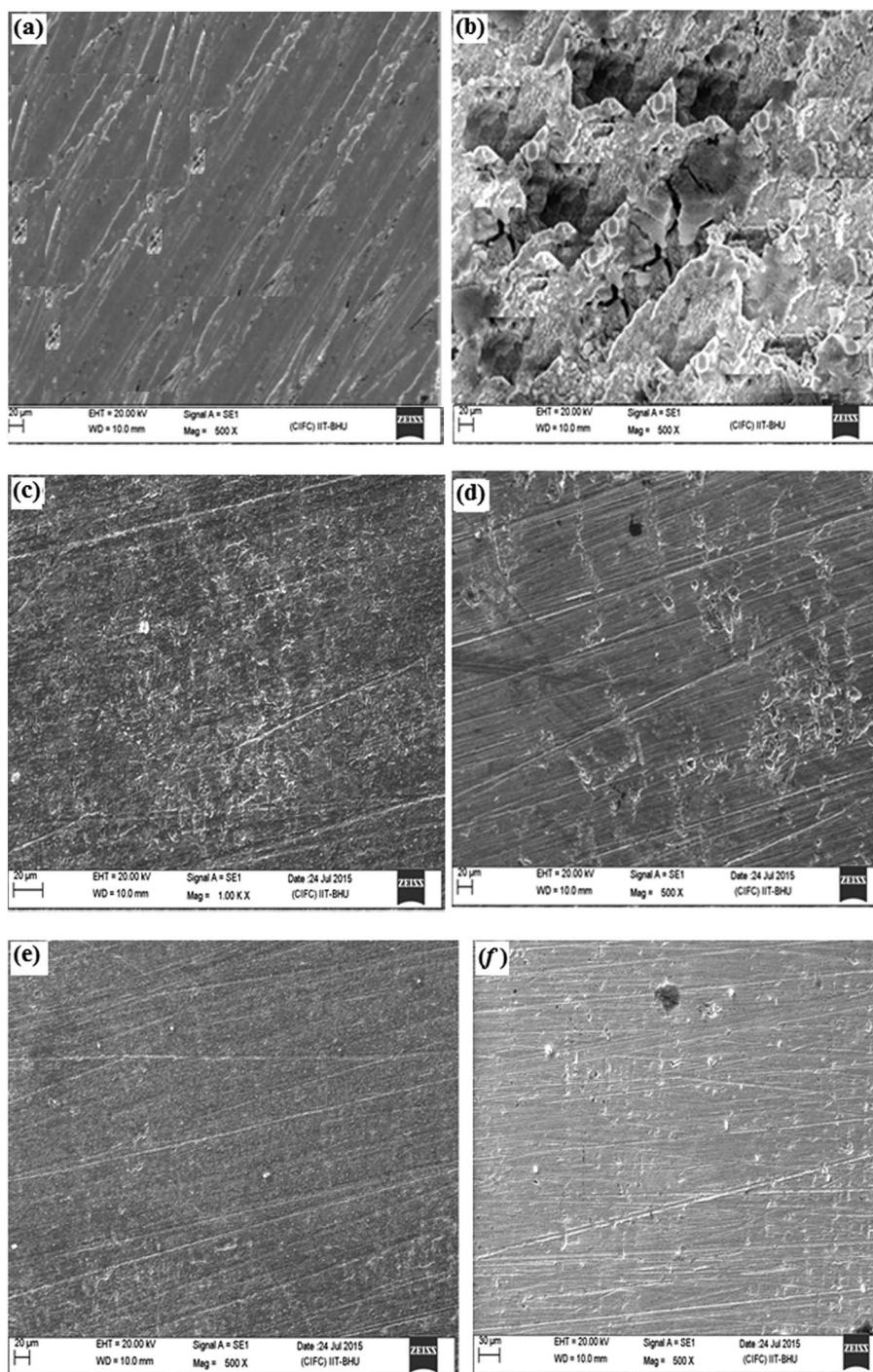
Fig. 7 SEM images of mild steel surfaces: abraded (a), in 1 M HCl in the absence of APQDs (b), and in 1 M HCl in the presence of 20 mg l^{-1} of **APQD-1** (c), **APQD-2** (d), **APQD-3** (e) and **APQD-4** (f).

charges,[79,80] and interaction of inhibitor molecules with the positively charged steel surface is a favorable process.

The Fukui indices, f_k^+ and f_k^- were calculated to predict the most probable atomic sites for nucleophilic and electrophilic attacks respectively. The electron density surfaces of the f_k^+ and f_k^- are shown in Fig. 10. The regions of the molecules with higher values of f_k^+ are more susceptible to attack by

electron rich species, while the sites of the molecules with higher values of f_k^- are more disposed to interactions with electron deficient species. It is apparent from the distributions of the differential change in electron density for the f_k^+ shown in Fig. 10 that the site of the nitro group in **APQD-1** is mostly likely to interact with negatively charged steel surface if such exists during the adsorption process, while the
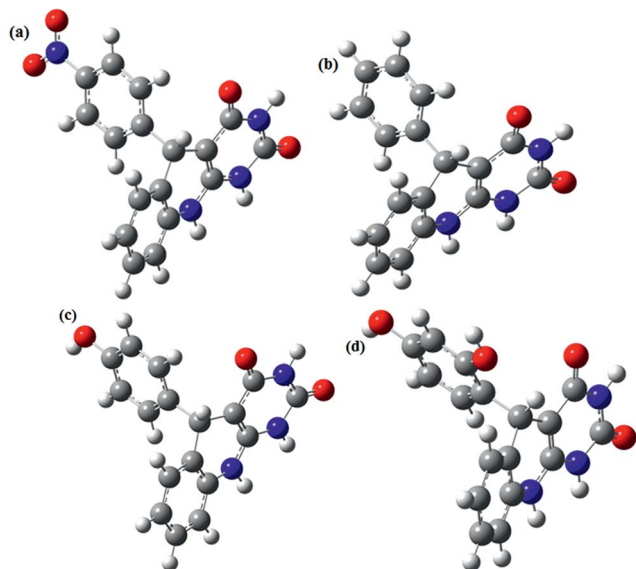
Fig. 8 Optimized molecular structures of (a) **APQD-1**, (b) **APQD-2**, (c) **APQD-3**, and (d) **APQD-4**.

corresponding most probable sites for possible interactions with negatively charged centers in **APQD-2**, **APQD-3** and **APQD-4** involve only some of the atoms in the pyrimido-quinoline-dione rings. The electron density surfaces for the f_k^- of the studied molecules also revealed that all the studied compounds have high tendencies of interacting with a positively charged iron surface *via* the pi-electron sites shared by the condensed pyrimido and the quinoline rings. The N- and O-atoms in the molecules except the nitro group in **APQD-1** also have good chances of nucleophilic interactions.

 3.4.2. Molecular dynamics (MD) simulations. The molecular dynamics simulations approach has emerged as a modern tool that aids the study of the interactions between inhibitor molecules and metal surface.[81] In the present study, the MD simulations studies were undertaken to predict the binding strength of the APQDs on the mild steel surface. Fig. 11 represents the side view equilibrium adsorption of all the studied inhibitors before and after molecular dynamics simulations. It can be seen from the Fig. 11 that all the studied compounds are adsorbed on mild steel surface with a flat or parallel orientation through several potential binding sites as previously pointed out in the quantum chemical study (*vide supra*). By considering that the Fe (110) surface is clean and ions free, the values of the interaction energy ($E_{interaction}$) and binding energy ($E_{binding}$) were calculated for all the studied inhibitors and the results are presented in Table 9. The results in Table 9 showed that the $E_{interaction}$ between the studied APQDs and Fe (110) surface are negative indicating spontaneous adsorption of the APQDs molecules on the Fe surface. A more negative value of $E_{interaction}$ between an organic molecule and a metal surface is a reflection of high $E_{binding}$.[82] Apparently, the high positive values of $E_{binding}$ for the investigated inhibitors indicate that the compounds adsorbed strongly on the Fe surface, which informs the experimentally observed high inhibition efficiency. The $E_{binding}$

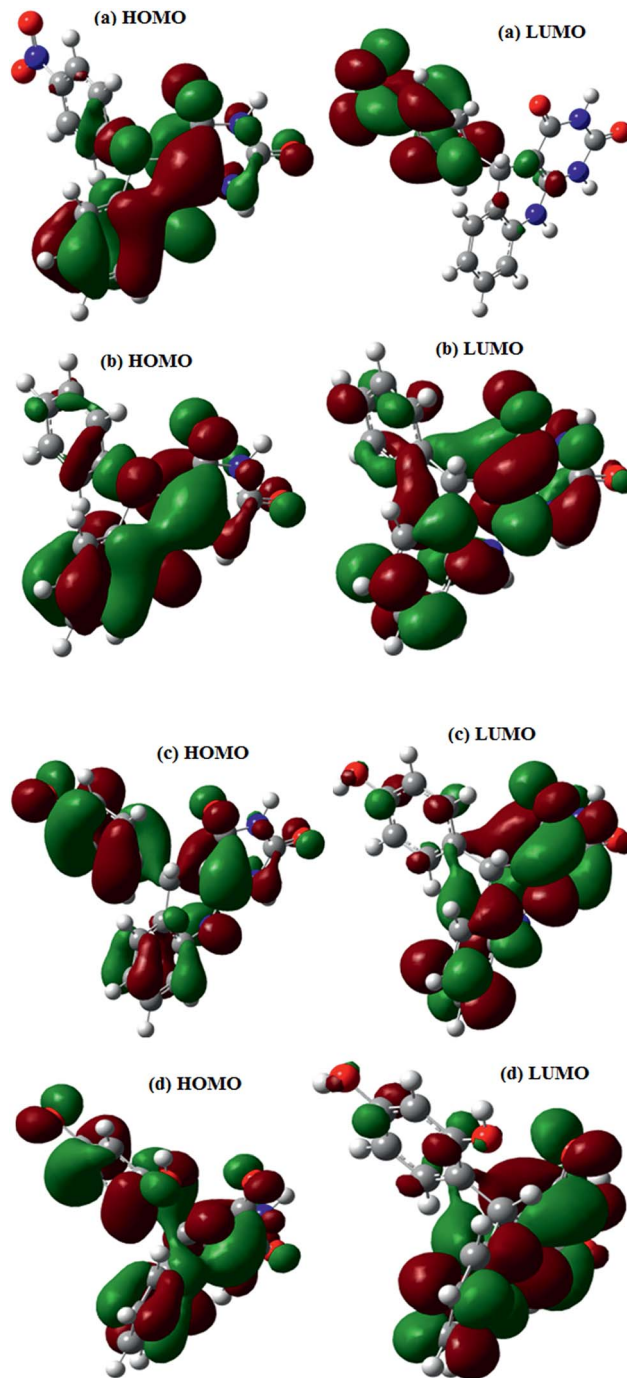**Fig. 9** The frontier molecular orbital (left-hand side: HOMO; and right-hand side: LUMO) of the studied APQDs (a) **APQD-1** (b) **APQD-2**, (c) **APQD-3**, and (d) **APQD-4**.

values (in kJ mol^{-1}) of the studied inhibitors follow the order: **APQD-4** (484.42) > **APQD-3** (448.94) > **APQD-2** (391.71) > **APQD-1** (349.11) which is in accordance with the order of the observed inhibition efficiency. The **APQD-4** gives the maximum value of $E_{binding}$ among all the four APQDs studied during whole simulation process suggesting that **APQD-4** adsorbed more efficiently on the mild steel surface and exhibited better inhibition efficiency than **APQD-3**, **APQD-2**, and **APQD-1**.[83]

Table 8 Quantum chemical parameters derived from the B3LYP/6-31+G(d,p) method

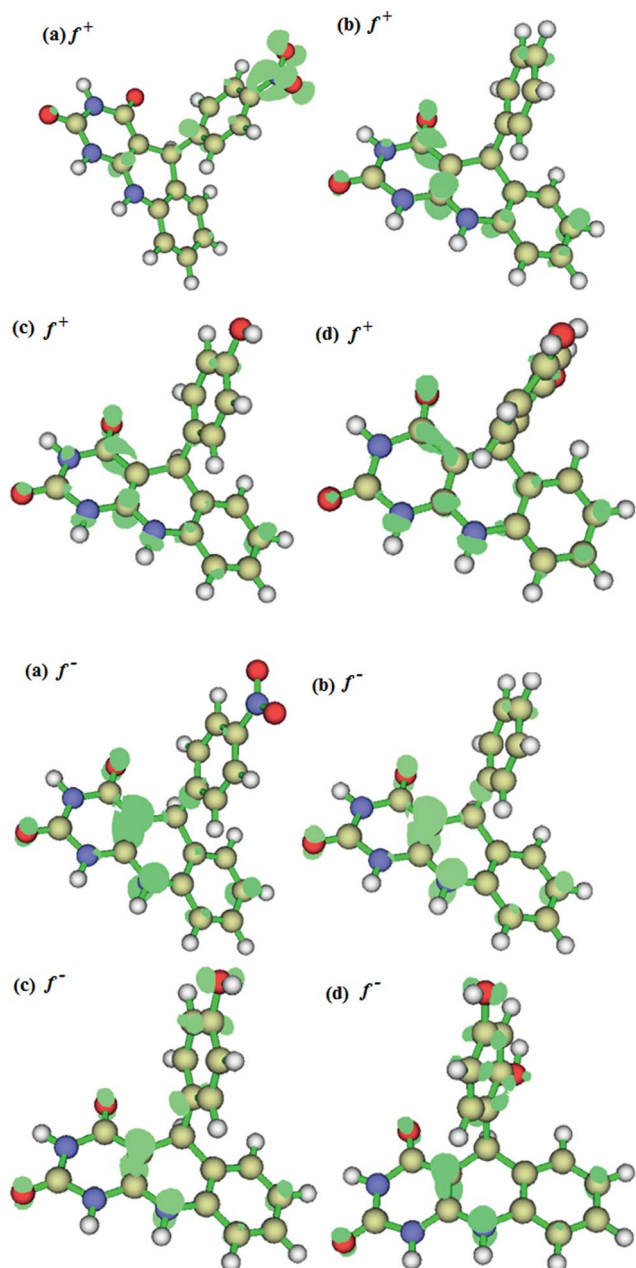| Compounds	Parameters				
	E_{HOMO} (eV)	E_{LUMO} (eV)	ΔE (eV)	χ (eV)	ΔN
APQD-1	−6.518	−2.763	3.755	4.640	0.629
APQD-2	−6.155	−1.316	4.838	3.735	0.675
APQD-3	−6.058	−1.282	4.776	3.670	0.697
APQD-4	−6.022	−1.173	4.848	3.598	0.702

Fig. 10 Fukui indices for the nucleophilic (f_k^+) and electrophilic (f_k^-) attacks for (a) **APQD-1**, (b) **APQD-2**, (c) **APQD-3**, and (d) **APQD-4** (all the surfaces were visualized at iso-surface value of 0.004, except for the f_k^+ of (c) **APQD-3**, and (d) **APQD-4** for which the isosurface value of 0.0028 and 0.0025 respectively were used for better visualization).
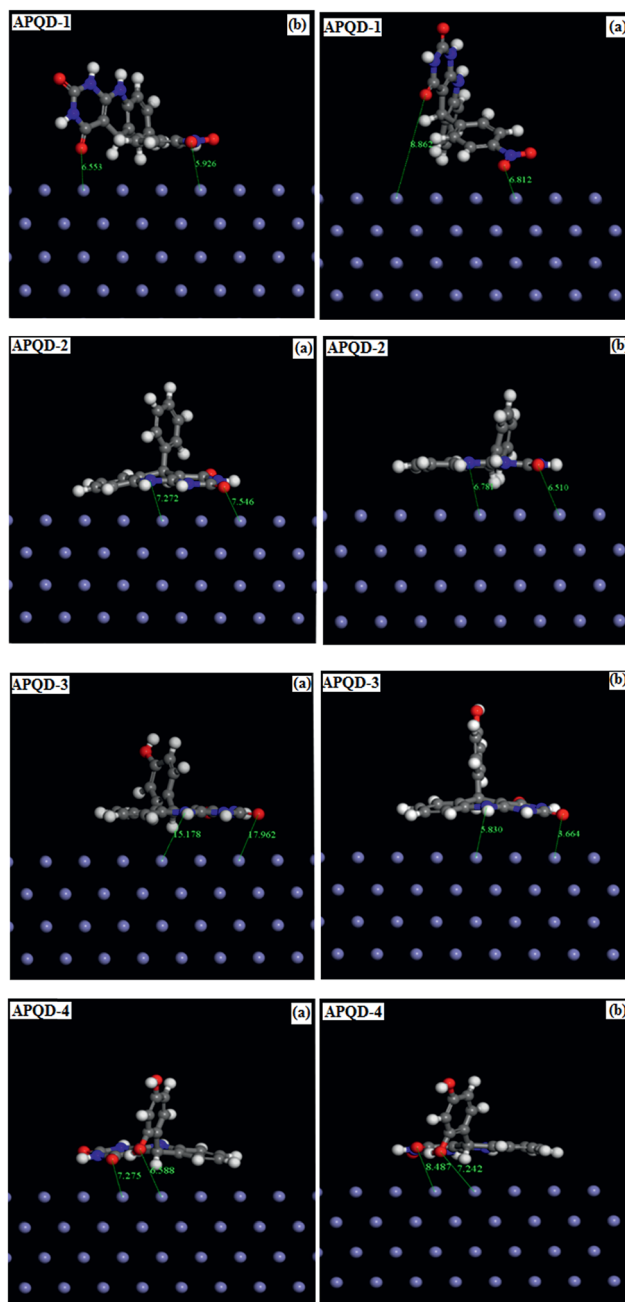

Fig. 11 Side view equilibrium adsorption of compound-1, compound-2, compound-3 and compound-4 on Fe (110) surface (a) before and (b) after molecular dynamics simulations.

Table 9 Interaction energies between the inhibitors and Fe (110) surface (in kJ mol^{-1})

Systems	$E_{interaction}$	$E_{binding}$
Fe(110) + **APQD-1**	−83.44	83.44
Fe(110) + **APQD-2**	−93.62	93.62
Fe(110) + **APQD-3**	−107.30	107.30
Fe(110) + **APQD-4**	−115.78	115.78

4. Conclusions

In the present study, the corrosion inhibition performances of four synthesized 5-arylpyrimido-[4,5-*b*]quinoline-diones (APQDs) were investigated for mild steel in 1 M HCl using experimental and theoretical methods and following conclusions were drawn:

(1) The 5-arylpyrimido-[4,5-*b*]quinoline-diones (APQDs) were found to inhibit the corrosion of mild steel in 1 M HCl and the inhibition efficiency increases with increasing concentration.

(2) EIS plots indicated that the charge transfer resistances increase with increasing concentration of the APQDs and maximum values were obtained at 20 mg l^{-1} concentration for each of the inhibitors.

(3) Potentiodynamic polarization study revealed that all the studied APQDs are mixed type inhibitors with predominant cathodic inhibition effects.

(4) Adsorption of the studied inhibitors on the mild steel surface obeys the Langmuir adsorption isotherm.

(5) Experimental and theoretical studies showed that presence of electron withdrawing group in **APQD-1** decreases the inhibition efficiency whereas presence of electron releasing –OH group(s) in **APQD-3** and **APQD-4** increases the inhibition efficiency.

(6) Quantum chemical calculations revealed that the mode of adsorption of the studied molecules on the steel surface is predominantly *via* electron donation from the high electron density sites of the molecules to the iron, and this is influenced by the nature of the substituent groups in the APQDs: the electron density of the HOMO is delocalized over the entire molecules in **APQD-3** and **APQD-4** due to presence of electron releasing –OH group(s) and the converse is true for **APQD-1** and **APQD-2**.

(7) The Fukui indices revealed the prospective sites for nucleophilic and electrophilic attacks in the studied APQDs such that the N- and O-atoms in the molecules except the nitro group in **APQD-1** showed high chances of nucleophilic interactions with charged metal surfaces.

(8) The MD simulations revealed that the studied compounds adsorbed on Fe surface in a flat or parallel orientation through several potential binding sites, and the calculated values of $E_{binding}$ are essentially high and assumed the same trend as the experimental inhibition efficiencies.

References

1 A. Yousefi, S. Javadian, N. Dalir, J. Kakemam and J. Akbari, *RSC Adv.*, 2015, **5**, 11697–11713.

2 M. Lebrini, M. Traisnel, M. Lagrene, B. Mernari and F. Bentiss, *Corros. Sci.*, 2007, **50**, 473–479.

3 L. C. Murulana, A. K. Singh, S. K. Shukla, M. M. Kabanda and E. E. Ebenso, *Ind. Eng. Chem. Res.*, 2012, **51**, 13282–13299.

4 L. C. Murulana, M. M. Kabanda and E. E. Ebenso, *RSC Adv.*, 2015, **5**, 28743–28761.

5 B. Hmamou, R. Salghi, A. Zarrouk, M. R. Aouad, O. Benali, H. Zarrok, M. Messali, B. Hammouti, E. E. Ebenso,

6 F. S. de Souza and A. Spinelli, *Corros. Sci.*, 2009, **51**, 642–649.

7 N. O. Eddy and E. E. Ebenso, *Afr. J. Pure Appl. Chem.*, 2008, **2**, 46–54.

8 O. K. Abiola, J. O. E. Otaigbe and O. J. Kio, *Corros. Sci.*, 2009, **51**, 1879–1881.

9 C. Beattie, M. North and P. Villuendas, *Molecules*, 2011, **16**, 3420–3432.

10 A. Domling, *Chem. Rev.*, 2006, **106**, 17–89.

11 M. S. Singh and S. Chowdhury, *RSC Adv.*, 2012, **2**, 4547–4592.

12 R. C. Cioc, E. Ruijter and R. V. A. Orru, *Green Chem.*, 2014, **16**, 2958–2975.

13 C. Capello, U. Fischer and K. Hungerbuhler, *Green Chem.*, 2007, **9**, 927–934.

14 H. Sharghi, R. Khalifeh and M. M. Doroodmand, *Adv. Synth. Catal.*, 2009, **351**, 207–218.

15 D. S. Bose, L. Fatima and H. B. Mereyala, *J. Org. Chem.*, 2003, **68**, 587–590.

16 N. R. Agrawal, S. P. Bahekar, P. B. Sarode, S. S. Zade and H. S. Chandak, *RSC Adv.*, 2015, **5**, 47053–47059.

17 T. P. Loh, L. C. Feng, H. Y. Yang and J. Y. Yang, *Tetrahedron Lett.*, 2002, **43**, 8741–8743.

18 R. A. Sheldon, *Green Chem.*, 2005, **7**, 267–278.

19 M. B. Deshmukh, S. M. Salunkhe, D. R. Patil and P. V. Anbhule, *Eur. J. Med. Chem.*, 2009, **44**, 2651–2654.

20 C. Oliver Kappe, *Eur. J. Med. Chem.*, 2000, **35**, 1043–1052.

21 M. M. Mojtahedi, M. R. Saidi, J. S. Shirzi and M. Bolourtchian, *Synth. Commun.*, 2002, **32**, 851–855.

22 E. E. Ebenso, I. B. Obot and L. C. Murulana, *Int. J. Electrochem. Sci.*, 2010, **5**, 1574–1586.

23 M. Singh and A. K. Bhattamishra, *J. Metall. Mater. Sci.*, 2007, **49**, 39–44.

24 L. Song-mei, Z. Hong-rui and L. Jian-hua, *Trans. Nonferrous Met. Soc. China*, 2007, **17**, 318–325.

25 N. Soltani, M. Behpour, E. E. Oguzie, M. Mahluji and M. A. Ghasemzadeh, *RSC Adv.*, 2015, **5**, 11145–11162.

26 N. Caliskan and E. Akbas, *Mater. Chem. Phys.*, 2011, **126**, 983–988.

27 F. M. Mahgoub, B. A. Abdel-Nabey and Y. A. El-Samadisy, *Mater. Chem. Phys.*, 2010, **120**, 104–108.

28 M. S. Masoud, M. K. Awad, M. A. Shaker and M. M. T. ElTahawy, *Corros. Sci.*, 2010, **52**, 2387–2396.

29 A. K. Nezhad, S. Sarikhani, E. S. Shahidzadeh and F. Panahi, *Green Chem.*, 2012, **14**, 2876–2884.

30 C. B. Verma, M. A. Quraishi and E. E. Ebenso, *Int. J. Electrochem. Sci.*, 2013, **8**, 7401–7413.

31 C. B. Verma, M. J. Reddy and M. A. Quraishi, *Anal. Bioanal. Electrochem.*, 2014, **6**, 321–340.

32 A. D. Becke, *J. Chem. Phys.*, 1993, **98**, 5648–5652.

33 A. D. Becke, *Phys. Rev. A*, 1988, **38**, 3098–3100.

34 C. Lee, W. Yang and R. G. Parr, *Phys. Rev. B: Condens. Matter Mater. Phys.*, 1988, **37**, 785–789.

35 M. J. Frisch, G. W. Trucks, H. B. Schlegel, G. E. Scuseria, M. A. Robb, J. R. Cheeseman, G. Scalmani, V. Barone, B. Mennucci and G. A. Petersson, *et al.*, *Gaussian 09, Revision D.01*, Gaussian, Inc., Wallingford CT, 2009.

M. Bouachrine and M. M. Kabanda, *Ind. Eng. Chem. Res.*, 2013, **52**, 14315–14327.

36 S. Martinez, *Mater. Chem. Phys.*, 2003, **77**, 97–102.

37 L. O. Olasunkanmi, I. B. Obot, M. M. Kabanda and E. E. Ebenso, *J. Phys. Chem. C*, 2015, **119**, 16004–16019.

38 R. G. Pearson, *Inorg. Chem.*, 1988, **27**, 734–740.

39 B. Gomez, N. V. Likhanova, M. A. Dominguez, R. Martinez-Palou, A. Vela and J. L. Gazquez, *J. Phys. Chem. B*, 2006, **110**, 8928–8934.

40 Y. Yan, X. Wang, Y. Zhang, P. Wang and J. Zhang, *Mol. Simul.*, 2013, **39**, 1034–1041.

41 W. Yang and W. J. Mortier, *J. Am. Chem. Soc.*, 1986, **108**, 5708–5711.

42 T. Lu and F. Chen, *J. Comput. Chem.*, 2012, **33**, 580–592.

43 T. Lu and F. Chen, *J. Mol. Graphics Modell.*, 2012, **38**, 314–323.

44 L. Guo, S. Zhu, S. Zhang, Q. He and W. Li, *Corros. Sci.*, 2014, **87**, 366–375.

45 I. B. Obot and Z. M. Gasem, *Corros. Sci.*, 2014, **83**, 359–366.

46 X. Jiang, Y. G. Zheng and W. Ke, *Corros. Sci.*, 2005, **47**, 2636–2658.

47 A. K. Satapathy, G. Gunasekaran, S. C. Sahoo, K. Amit and P. V. Rodrigues, *Corros. Sci.*, 2009, **51**, 2848–2856.

48 G. Gunasekaran and L. R. Chauhan, *Electrochim. Acta*, 2004, **49**, 4387–4395.

49 D. K. Yadav and M. A. Quraishi, *Ind. Eng. Chem. Res.*, 2012, **51**, 14966–14979.

50 C. Verma, M. A. Quraishi and A. Singh, *J. Taiwan Inst. Chem. Eng.*, 2015, 1–14.

51 P. M. Wadhwani, D. G. Ladha, V. K. Panchal and N. K. Shah, *RSC Adv.*, 2015, **5**, 7098–7111.

52 L. Bai, L. Feng, H. Wang, Y. Lu, X. Lei and F. Bai, *RSC Adv.*, 2015, **5**, 4716–4726.

53 C. Verma, P. Singh, I. Bahadur, E. E. Ebenso and M. A. Quraishi, *J. Mol. Liq.*, 2015, **209**, 767–778.

54 C. B. Verma, M. A. Quraishi and E. E. Ebenso, *Int. J. Electrochem. Sci.*, 2013, **8**, 12894–12906.

55 G. M. Schmid and H. J. Huang, *Corros. Sci.*, 1980, **20**, 1041–1057.

56 I. B. Obot, N. O. Obi-Egbedi and S. A. Umoren, *Int. J. Electrochem. Sci.*, 2009, **4**, 863–877.

57 R. Karthikaiselvi and S. Subhashini, *J. Assoc. Arab Univ. Basic Appl. Sci.*, 2014, **16**, 74–82.

58 E. E. Oguzie, B. N. Okolue, E. E. Ebenso, G. N. Onuoha and A. I. Onuchukwu, *Mater. Chem. Phys.*, 2004, **87**, 394–401.

59 S. Ghareba and S. Omanovic, *Corros. Sci.*, 2010, **52**, 2104–2113.

60 C. M. Goulart, A. Esteves-Souza, C. A. Martinez-Huitle, C. J. F. Rodrigues, M. A. M. Maciel and A. Echevarria, *Corros. Sci.*, 2013, **67**, 281–291.

61 M. A. Amin and M. M. Ibrahim, *Corros. Sci.*, 2011, **53**, 873–885.

62 S. Issaadi, T. Douadi, A. Zouaoui, S. Chafaa, M. A. Khan and G. Bouet, *Corros. Sci.*, 2011, **53**, 1484–1488.

63 M. A. Amin, M. A. Ahmed, H. A. Arida, T. Arslan, M. Saraçoglu and F. Kandemirli, *Corros. Sci.*, 2011, **53**, 540–548.

64 F. Bentiss, M. Lebrini and M. Lagrenee, *Corros. Sci.*, 2005, **47**, 2915–2931.

65 R. Yıldız, T. Dogan and I. Dehri, *Corros. Sci.*, 2014, **85**, 215–221.

66 P. Mourya, S. Banerjee and M. M. Singh, *Corros. Sci.*, 2014, **85**, 352–363.

67 R. Solmaz, *Corros. Sci.*, 2014, **81**, 75–84.

68 M. Chevalier, F. Robert, N. Amusant, M. Traisnel, C. Roos and M. Lebrini, *Electrochim. Acta*, 2014, **131**, 96–105.

69 P. Roy, P. Karfa, U. Adhikari and D. Sukul, *Corros. Sci.*, 2014, **88**, 246–253.

70 C. Verma, P. Singh and M. A. Quraishi, *J. Assoc. Arab Univ. Basic Appl. Sci.*, 2015, DOI: 10.1016/j.jaubas.2015.04.003.

71 A. Yousefi, S. Javadian, N. Dalir, J. Kakemam and J. Akbari, *RSC Adv.*, 2015, **5**, 11697–11713.

72 C. Verma, A. Singh, G. Pallikonda, M. Chakravarty, M. A. Quraishi, I. Bahadur and E. E. Ebenso, *J. Mol. Liq.*, 2015, **209**, 306–319.

73 P. Roy, P. Karfa, U. Adhikari and D. Sukul, *Corros. Sci.*, 2014, **88**, 246–253.

74 C. Verma, M. A. Quraishi and A. Singh, *J. Taiwan Inst. Chem. Eng.*, 2015, **49**, 229–239.

75 E. E. Ebenso, M. M. Kabanda, L. C. Murulana, A. K. Singh and S. K. Shukla, *Ind. Eng. Chem. Res.*, 2012, **51**, 12940–12958.

76 F. Chiter, C. Lacaze-Dufaure, H. Tangb and N. Pebere, *Phys. Chem. Chem. Phys.*, 2015, **17**, 22243–22258.

77 M. Lebrini, M. Lagrenee, H. Vezin, L. Gengembre and F. Bentiss, *Corros. Sci.*, 2005, **47**, 485–505.

78 L. Herrag, B. Hammouti, S. Elkadiri, A. Aouniti, C. Jama and H. Vezin, *Corros Sci.*, 2010, **2010**(52), 3042–3051.

79 S. K. Saha, A. Dutta, P. Ghosh, D. Sukulc and P. Banerjee, *Phys. Chem. Chem. Phys.*, 2015, **17**, 5679–5690.

80 C. Verma, M. A. Quraishi, L. O. Olasunkanmibc and E. E. Ebenso, *RSC Adv.*, 2015, **5**, 85417–85430.

81 B. Xu, W. Yang, Y. Liu, X. Yin, W. Gong and Y. Chen, *Corros. Sci.*, 2014, **78**, 260–268.

82 S. John, J. Joy, M. Prajila and A. Joseph, *Mater. Corros.*, 2011, **62**, 1031–1041.

83 L. O. Olasunkanmi, I. B. Obot, M. M. Kabanda and E. E. Ebenso, *J. Phys. Chem. C*, 2015, **119**, 16004–16019.